Mechanics of Materials 188 (2024) 104864

Contents lists available at ScienceDirect

Mechanics of Materials

journal homepage: www.elsevier.com/locate/mecmat

Research paper

The viscoelastic behavior of lignin: Quantification through nanoindentation relaxation testing on hot-pressed technical lignin samples from various origins

Michael Schwaighofer [a,*], Markus Königsberger [a], Luis Zelaya-Lainez [b], Markus Lukacevic [b], Sebastián Serna-Loaiza [c], Michael Harasek [c], Florian Zikeli [d], Anton Friedl [c], Josef Füssl [b]

[a] Institute for Mechanics of Materials and Structures, TU Wien, Karlsplatz 13/202, 1040, Vienna, Austria
[b] Christian Doppler Laboratory for Next-Generation Wood-Based Biocomposite, Institute for Mechanics of Materials and Structures, TU Wien, Karlsplatz 13/202, 1040, Vienna, Austria
[c] Christian Doppler Laboratory for Next-Generation Wood-Based Biocomposite, Institute of Chemical, Environmental and Bioscience Engineering, TU Wien, Getreidemarkt 9/166, 1040, Vienna, Austria
[d] Department for Innovation in Biological Systems, Agriculture and Food, University of Tuscia, Via S.M. in Gradi n.4, Viterbo, 01100, Italy

ARTICLE INFO

Keywords:
Creep
Rheology
Functional equations
Homogenization
Biopolymer
Wood

ABSTRACT

Lignin, the second most abundant organic polymer on earth, is one of the primary causes of the viscoelastic behavior of plants. An accurate characterization of its viscoelastic properties is essential for predicting the time-dependent response of natural materials, including wood and plant fibers, and for advancing lignin-based materials and their production methods, such as 3D printing of biocomposites. To enrich the still rather sparse knowledge on the viscoelasticity of lignin, we re-evaluate nanoindentation relaxation tests performed on five hot-pressed technical lignins extracted from different feedstocks, using three different extraction methods. The viscoelastic indentation problem is addressed using the method of functional equations combined with the homogenization theory to account for the production-induced porosity. This evaluation procedure allows for quantitatively assessing the viscoelastic properties of lignin, which can be very accurately described by an isochoric four-parameter Burgers model. Remarkably, the viscoelastic properties of all tested lignins are practically identical and independent of the feedstock and the extraction processes.

1. Introduction

Lignin is, after cellulose, the second most common organic polymer on the planet (Watkins et al., 2015; Windeisen and Wegener, 2012). It is mainly found as part of the cell walls of plants (Plomion et al., 2001), where it forms lignin–carbohydrate complexes together with hemicellulose (Watkins et al., 2015). Most of the so-called technical lignin is a byproduct of the delignification processes adopted in the pulp and paper-making industry (Windeisen and Wegener, 2012), making lignin accessible in large quantities and in relatively pure form. While a majority of the technical lignin is currently used as an energy source, recent efforts have focused on valorizing lignin in more demanding applications (Bajwa et al., 2019; Tuck et al., 2012) such as the production of more sustainable composite materials (Lee et al., 2015), carbon fibers (Baker et al., 2012), asphalts (Xu et al., 2017), plastics (Hilburg et al., 2014), and electrospun lignin mats for lubricating applications (Rubio-Valle et al., 2023). The emergence of new lignin-based composite materials is additionally fostered by the rapid progress in additive manufacturing technologies. Lignin can be made 3D printable after blending or copolymerization (Ebers et al., 2021). To facilitate the development of lignin-based materials, particularly when 3D printed, understanding the mechanical properties of technical lignin is vital.

Like many other natural polymers including collagen (Puxkandl et al., 2002; Tian et al., 2022) or natural rubber (Amin et al., 2002; Hagen et al., 1996), lignin is often considered to be a viscoelastic material, entailing that it responds with both instantaneous elastic and continuously increasing viscous deformations (creep) to applied and sustained stresses and, similarly, that it responds with both instantaneous (elastic) and continuously decreasing viscous stresses (relaxation) to applied and sustained deformations. Lignin and hemicellulose appear to be the cause of the viscoelastic behavior of plants (Eitelberger et al., 2012; Habibi et al., 2016; Olsson and Salmén, 1992; Salmén, 1984). Therefore, comprehending the viscoelastic behavior of lignin contributes to

* Corresponding author.
E-mail address: michael.schwaighofer@tuwien.ac.at (M. Schwaighofer).

https://doi.org/10.1016/j.mechmat.2023.104864
Received 14 July 2023; Received in revised form 5 October 2023; Accepted 6 November 2023
Available online 8 November 2023

the understanding and modeling of natural lignin-based materials such as plant fibers (Königsberger et al., 2023), wood (Eitelberger et al., 2012), and bamboo (Gangwar and Schillinger, 2019).

The elastic properties of lignin are relatively well-known. The elastic modulus depends strongly on the moisture content (Cousins, 1976; Hess et al., 2018; Marcuello et al., 2020) and the oxidation state of lignin (Marcuello et al., 2020). The modulus of hot-pressed technical lignin is, however, independent of the extraction process and feedstock, if production-induced porosity is accounted for (Schwaighofer et al., 2023).

Unfortunately, much less is known regarding the viscous behavior of lignin. Experimental evidence of the viscoelastic nature of lignin mainly stems from testing natural wood either by means of classical macroscopic creep tests (Akter et al., 2023; Hofer et al., 2019; Salmén, 1984) or by means of nanoindentation tests in wood cells (Gindl et al., 2004; Zhang et al., 2012). More recently, the viscoelastic nature of pure technical lignin has been observed in a large nanoindentation test campaign (Schwaighofer et al., 2023). Further evidence comes from experimental observations that adding technical lignin to asphalt (Xu et al., 2017) and to hydrogels (Bian et al., 2018) increases the viscoelastic behavior of the composite material. Despite these qualitative findings, the viscoelastic behavior of lignin has, to the authors' knowledge, never been quantified experimentally. One molecular dynamics nanoseconds long creep simulation of a lignin molecule was performed, noticing a Maxwell-like creep behavior (Habibi et al., 2016). Only one other indirect quantification attempt exists (Eitelberger et al., 2012), which employs micromechanics multiscale modeling to calibrate the viscoelastic behavior of a lignin–hemicellulose phase from macroscopic creep tests on clearwood (Schniewind and Barrett, 1972). This multiscale model considered the lignin–hemicellulose phase as the origin of creep of wood and is able to successfully model the viscoelastic behavior of clearwood.

In this paper, we aim to close this knowledge gap by quantifying the viscoelastic properties of technical lignin. Therefore, we re-evaluate the nanoindentation tests performed by Schwaighofer et al. (2023), in a displacement-controlled mode with a trapezoid load path giving us access to a large number of relaxation tests. Considering lignin as an isotropic linear viscoelastic material, an analytical solution of the respective indentation problem with a conical indenter tip based on the method of functional equations (Lee and Radok, 1960; Radok, 1957) is available (Vandamme and Ulm, 2006). Homogenization theory is used in combination with the method of the functional equations (Davydov and Jirásek, 2008) to translate the measured indentation results to the solid part of the hot-pressed technical lignin and thus account for the effect of unavoidable production-induced porosity in the samples. This solution is then fitted to the holding phase of the nanoindentation relaxation tests to quantify, for the first time, the viscoelastic properties of solid pore-free lignin. Nanoindentation tests are available for five technical lignins extracted from softwood, hardwood, and grass by means of organosolv, kraft pulping, and enzyme hydrolysis. This way, we additionally aim at studying whether the different chemical properties of the technical lignins—in more detail the different phenylpropane units and linkages found in lignins from different origin (Chio et al., 2019; Watkins et al., 2015; Windeisen and Wegener, 2012), and/or the chemical differences related to the extraction method (Asawaworarit et al., 2019; Windeisen and Wegener, 2012)—translate into different viscoelastic properties.

2. Materials and methods

2.1. Raw materials and specimen preparation

The nanoindentation tests from Schwaighofer et al. (2023), which are the foundation for determining the viscoelastic properties of hot-pressed lignin, are shortly summarized in this section. Five lignins were examined, obtained from three different feedstocks and extraction techniques. Two lignins originated from softwood (SW), two lignins from hardwood (HW), and one from grass (G). The lignins were extracted using kraft pulping (K), organosolv processing (OS), and enzymatic hydrolysis (E). Correspondingly, the five lignins were labeled E-HW, OS-G, OS-HW, OS-SW, and K-SW, see Table 1. The Klason lignin, ash, and carbohydrate content were determined as acid-soluble lignin (ASL) and acid-insoluble lignin (AIL) according to the NREL/TP-510–42618 (Sluiter et al., 2012). Four of the five lignins had approximately 90 wt.% lignin content, except for K-SW, which had a significantly lower Klason lignin content. Furthermore, all lignins except E-HW had carbohydrate contents below 1.3 wt.%. Due to differences in the feedstock used for extraction, the chemical profile of each lignin varied in terms of the conforming monolignols like hydroxy phenol (H), guaiacyl (G), and syringyl (S) units. Thus, the respective H/G/S ratios and Klason analysis results indicate that all used lignins had different chemical structures and compositions.

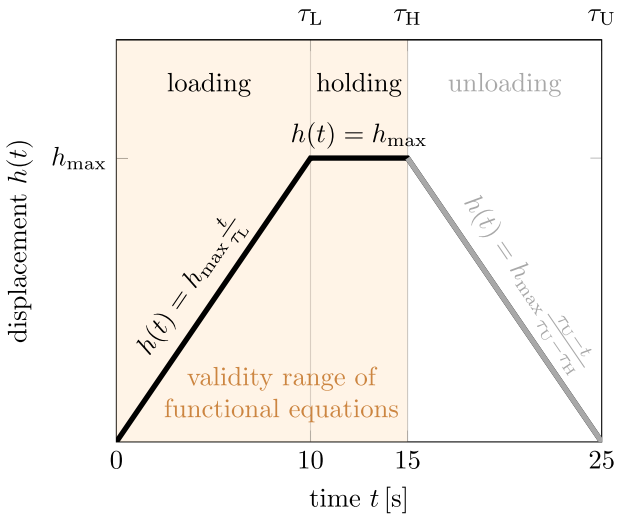

Fig. 1. Trapezoidal displacement-controlled loading path.

The extracted lignin powder was pressed into disks with a pressure of 108 MPa at 90 °C. The disks were split in half along the central plane, and the resulting middle surface was smoothed until the (root mean square) surface roughness was below 40 nm, see Table 1 for details. The specimens were stored and tested at constant climatic conditions characterized by a relative humidity of 35% and a temperature 21 °C, respectively.

2.2. Grid nanoindentation testing

Nanoindentation tests were performed using a Hysitron TI900 Tribolindenter with a diamond Berkovich tip in displacement-controlled mode. Out of the several grids tested, those referring to maximum indentation depths h_{max} of 600 nm, 900 nm, and 1000 nm were considered reliable, while tests at smaller depth revealed strong size effects. Tests at larger depths led to pronounced damage. A total of 6300 indentation tests with at least 100 indents per indentation depth were performed, see Table 1 for details regarding the grids. The trapezoidal displacement history (see Fig. 1) of each nanoindentation test was defined as follows:

$$h(t) = \begin{cases} h_{max} \frac{t}{\tau_L} & \forall \quad 0 \le t \le \tau_L \\ h_{max} & \forall \quad \tau_L \le t \le \tau_H \\ h_{max} \frac{\tau_U - t}{\tau_U - \tau_H} & \forall \quad \tau_H \le t \le \tau_U \end{cases}, \tag{1}$$

where $\tau_L = 10$ s, $\tau_H = 15$ s and $\tau_U = 25$ s were the times at the end of loading, holding, and unloading, respectively.

Table 1
Parameters of the lignin specimens: extraction process, feedstock, chemical composition, monolignol ratios, surface roughness, porosity, and nanoindentation grid size per indentation depth (Schwaighofer et al., 2023).

	Extraction process	Feedstock category	Klason lignin [wt.%]	Ash [wt.%]	Carbohydrates [wt.%]	H/G/S ratio [%] (Henriksson, 2009)	Surface roughness [nm]	Porosity φ [%]	Grid per indentation depth
E-HW	Enz. Hydrolysis	Hardwood	86.44	0.08	8.51	0-8/25-50/46–75	25	13.7	$4 \times 5 \times 5$
OS-G	Organosolv	Grass	93.70	1.60	0.52	5-33/33-80/20–54	40	56.2	$2 \times 10 \times 10$
OS-HW	Organosolv	Hardwood	88.39	0.00	0.60	0-8/25-50/46–75	21	22.0	$4 \times 5 \times 5$
OS-SW	Organosolv	Softwood	90.04	0.12	1.08	0-5/95-99/0	25	35.5	40 × 40
K-SW	Kraft pulping	Softwood	17.57	66.37	1.24	0-5/95-99/0	30	6.5	10 × 10

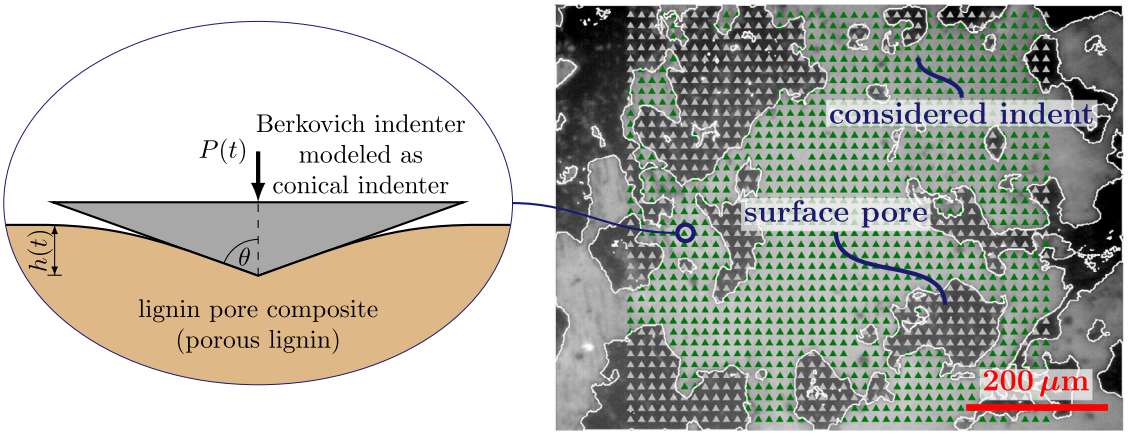

Fig. 2. Representative light microscopy image of OS-SW lignin, on which the identified surface porosity (dark areas outlined in white) and the 40 × 40 indentation grid are mapped. Grids inside the surface porosity (gray triangles) are eliminated, only the indents in polished regions (green triangles) are considered for evaluation.

2.3. Image analysis and porosity determination

Hot-pressing of lignin powder resulted in a porous microstructure. The sample-specific porosity φ was determined from two light microscopy images, by calculating the ratio of the surface area of the pores (identified with an adaptive gray level threshold) to the total area of the images. The porosity varies considerably among the different lignins, from 6.5% to 56.2% (Schwaighofer et al., 2023), see Table 1 for all porosity values and Fig. 2 for a representative light microscopy image. Density measurements confirmed that the surface porosity is indeed representative of the bulk porosity. Since regions of the surface pores breach the requirement of a flat and smooth surface (Donnelly et al., 2006), only the indents outside the surface pores (green points in Fig. 2) are considered reliable in the remainder of this study.

2.4. Determination of outliers and averaging

Nanoindentation relaxation tests measure the force evolutions (relaxation curves) and are available for each grid point (located outside the surface pore regions), for each of the five lignins, and for each of the three considered indentation depths, see Fig. 3 for all relaxation curves of E-HW lignin at $h_{\max} = 900\,\text{nm}$. Most probably due to defects or other heterogeneities in the probed domain, some of the measured relaxation curves are not dictated by the bulk material behavior. They are therefore considered outliers, whereby two criteria for outlier detection are formulated:

- Indents with either unexpectedly low forces (material response too soft) or high forces (material response too stiff) are removed by the criterion that, the corresponding indentation modulus (determined by the classical Oliver and Pharr (1992) method) has to fall in between the lower quartile minus 1.5 times the interquartile range and the upper quartile plus 1.5 times the interquartile range (Schwaighofer et al., 2023).
- Indents with unexpected relaxation curve shapes, particularly with force drops during the loading, are removed. A force drop is identified by a sudden change in the gradient dP/dt, which can be best recognized through significant variations in the curvature d^2P/dt^2. Consequently, only curves with a coefficient of variation of the curvature during the loading phase ($0 \le t \le \tau_L$) below 10 are considered acceptable.

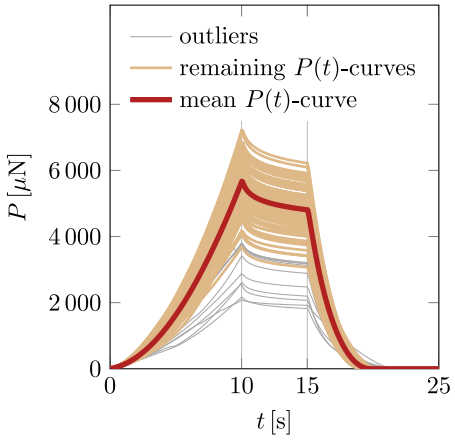

Fig. 3. Representative (lignin: E-HW, $h_{\max} = 900\,\text{nm}$) considered relaxation curves ($P(t)$-curves) and their average as well as the removed outliers.

With these two methods, on average 9% of the relaxation curves are removed for each lignin and indentation depth. From the remaining indents, a mean relaxation curve ($P(t)$-curve) and a mean Oliver–Pharr indentation modulus E^r are calculated, see Fig. 3. These mean values are used in the remainder of the paper.

2.5. Elastic homogenization — solid and porous lignin

We aim at back-calculating the relaxation properties of solid lignin, i.e., pore-free lignin, from the nanoindentation-measured relaxation curves. Schwaighofer et al. (2023) demonstrated that almost all the

indents, even the ones seemingly "far" away from the surface pore regions, still "feel" the pores, i.e., the indentation tests probe the lignin-pore composite material rather than the solid lignin material. Hence, we understand the measured force evolutions as the response of a lignin-pore composite. Classical homogenization theory is employed to upscale the elastic properties from the solid lignin to the porous lignin, as detailed next. The elastic upscaling rule will then be used for solving the viscoelastic indentation problem.

Given the obvious matrix-inclusion morphology (Fig. 2), the Mori–Tanaka (Benveniste, 1987; Mori and Tanaka, 1973) homogenization scheme is employed. The pores are considered as spherical inclusions with vanishing stiffness to be embedded in an isotropic matrix phase of solid lignin with bulk modulus K_{sl} and shear modulus G_{sl}. The corresponding bulk and shear moduli of porous lignin (K_{pl} and G_{pl}) are then also isotropic and read as:

$$K_{\mathrm{pl}} = \frac{4G_{\mathrm{sl}}K_{\mathrm{sl}}(1-\varphi)}{4G_{\mathrm{sl}}+3K_{\mathrm{sl}}\varphi}\,, \tag{2}$$

$$G_{\mathrm{pl}} = \frac{G_{\mathrm{sl}}(1-\varphi)(8G_{\mathrm{sl}}+9K_{\mathrm{sl}})}{8G_{\mathrm{sl}}+9K_{\mathrm{sl}}+(12G_{\mathrm{sl}}+6K_{\mathrm{sl}})\varphi}\,. \tag{3}$$

We are interested in an expression of the indentation modulus of porous lignin. Assuming a rigid indenter tip, the indentation modulus of porous lignin, $E^{\mathrm{i}}_{\mathrm{pl}}$, can be expressed as a function of the Young's modulus E_{pl} and the Poisson's ratio ν_{pl} as (Oliver and Pharr, 1992):

$$E^{\mathrm{i}}_{\mathrm{pl}} = \frac{E_{\mathrm{pl}}}{1-\nu^2_{\mathrm{pl}}}\,. \tag{4}$$

By applying the following relation for isotropic materials,

$$G_{\mathrm{pl}} = \frac{E_{\mathrm{pl}}}{2(1+\nu_{\mathrm{pl}})} \quad \text{and} \quad K_{\mathrm{pl}} = \frac{E_{\mathrm{pl}}}{3(1-2\nu_{\mathrm{pl}})}\,, \tag{5}$$

the indentation modulus can also be written as a function of the shear modulus G_{pl} and bulk modulus K_{pl} (Vandamme and Ulm, 2006) as:

$$E^{\mathrm{i}}_{\mathrm{pl}} = 4G_{\mathrm{pl}}\frac{3K_{\mathrm{pl}}+G_{\mathrm{pl}}}{3K_{\mathrm{pl}}+4G_{\mathrm{pl}}}\,. \tag{6}$$

Inserting Eqs. (2) and (3) in the indentation modulus expression Eq. (6) results in the sought expression of the indentation modulus of porous lignin as a function of the solid lignin stiffness constants, reading as:

$$E^{\mathrm{i}}_{\mathrm{pl}} = \frac{G_{\mathrm{sl}}(1-\varphi)(8G_{\mathrm{sl}}+9K_{\mathrm{sl}})[32G^2_{\mathrm{sl}}+9K^2_{\mathrm{sl}}(12+11\varphi)+12G_{\mathrm{sl}}K_{\mathrm{sl}}(11+14\varphi)]}{(4G_{\mathrm{sl}}+3K_{\mathrm{sl}})(8G_{\mathrm{sl}}+9K_{\mathrm{sl}}+12G_{\mathrm{sl}}\varphi+6K_{\mathrm{sl}}\varphi)[8G_{\mathrm{sl}}+3K_{\mathrm{sl}}(3+5\varphi)]}\,. \tag{7}$$

2.6. Estimating viscoelastic properties of lignin — Method of functional equations

Solid lignin is considered to be a linear viscoelastic and isotropic material. Following the homogenization approach of the previous subsection, this is also the case for porous lignin. Stresses $\boldsymbol{\sigma}$ and strains $\boldsymbol{\varepsilon}$ of solid and porous lignin, respectively, are therefore linked by the relaxation function $R(t)$ according to Boltzmann's superposition principle (Lakes, 1998) reading as:

$$\boldsymbol{\sigma}^{\mathrm{vol}}(t) = 3\int_0^t R^{\mathrm{vol}}(t-\tau)\mathbb{I}^{\mathrm{vol}} : \frac{\mathrm{d}}{\mathrm{d}\tau}\boldsymbol{\varepsilon}^{\mathrm{vol}}(\tau)\mathrm{d}\tau \tag{8}$$

$$\boldsymbol{\sigma}^{\mathrm{dev}}(t) = 2\int_0^t R^{\mathrm{dev}}(t-\tau)\mathbb{I}^{\mathrm{dev}} : \frac{\mathrm{d}}{\mathrm{d}\tau}\boldsymbol{\varepsilon}^{\mathrm{dev}}(\tau)\mathrm{d}\tau \tag{9}$$

with the decoupling rules $\boldsymbol{\sigma} = \boldsymbol{\sigma}^{\mathrm{vol}} + \boldsymbol{\sigma}^{\mathrm{dev}}$ and $\boldsymbol{\varepsilon} = \boldsymbol{\varepsilon}^{\mathrm{vol}} + \boldsymbol{\varepsilon}^{\mathrm{dev}}$. $\mathbb{I}^{\mathrm{vol}}$ and $\mathbb{I}^{\mathrm{dev}}$ stand for the volumetric and deviatoric parts of the symmetric fourth-order identity tensor. The Laplace transformation of Eqs. (8) and (9) changes the convolution integral into an algebraic formulation

$$\widehat{\boldsymbol{\sigma}^{\mathrm{vol}}(s)} = 3\underbrace{\widehat{R^{\mathrm{vol}}(s)}s}_{\widehat{K(s)}}\mathbb{I}^{\mathrm{vol}} : \widehat{\boldsymbol{\varepsilon}^{\mathrm{vol}}(s)} \tag{10}$$

$$\widehat{\boldsymbol{\sigma}^{\mathrm{dev}}(s)} = 2\underbrace{\widehat{R^{\mathrm{dev}}(s)}s}_{\widehat{G(s)}}\mathbb{I}^{\mathrm{dev}} : \widehat{\boldsymbol{\varepsilon}^{\mathrm{dev}}(s)} \tag{11}$$

where $\widehat{\bullet(s)}$ donates the Laplace transform according to

$$\widehat{f(s)} = \int_0^\infty f\exp(-st)\mathrm{d}t\,, \tag{12}$$

with the complex variable s.

To characterize the viscoelastic behavior, we aim at quantifying a relaxation function of (solid) lignin R_{sl} from the measured mean relaxation curves, for each indentation depth and each lignin type. Then, the sought relaxation function can be deduced by applying the method of functional equations developed by Radok (1957) and Lee and Radok (1960) and commonly used for identifying viscoelastic properties from nanoindentation tests (Ahmad et al., 2010; Ashrafi and Shariyat, 2010; Davydov and Jirásek, 2008; Huang and Lu, 2007; Jäger et al., 2007; Kariem et al., 2020; Lu et al., 2003; Vandamme and Ulm, 2006). Notably, the method of functional equations is essential for indentation problems, where the boundary conditions vary due to the time-dependent contact area between the indenter and indented material. Therefore the viscoelastic indentation problem cannot be solved by the classical viscoelastic correspondence principle (Radok, 1957), which is limited to time-invariant boundary conditions.

First, a simple linear elastic indentation problem in an isotropic homogeneous half-space of porous lignin is considered. Modeling the Berkovich indenter as a rigid cone with a half-angle θ of 70.3° (see Fig. 2) allows us to use Sneddon's classical relationship between the indentation force P and the indentation depth h reading as (Sneddon, 1965):

$$P(t) = \frac{2\tan\theta}{\pi}E^{\mathrm{i}}_{\mathrm{pl}}(K_{\mathrm{sl}},G_{\mathrm{sl}},\varphi)\,h^2(t)\,. \tag{13}$$

Then we extend the purely elastic indentation problem to a viscoelastic indentation problem by exploiting the method of functional equations, summarized hereafter. The elastic constant in Sneddon's elastic solution Eq. (13), i.e., the two elastic isotropic constants of solid lignin, K_{sl} and G_{sl} in the indentation modulus $E^{\mathrm{i}}_{\mathrm{pl}}$ Eq. (7), are replaced by their corresponding viscoelastic differential operators (Radok, 1957), yielding a so-called functional equation of the viscoelastic indentation problem. This equation can be mathematically conveniently realized and solved after the Laplace transformation—resulting in the following algebraic equation in the Laplace domain Vandamme and Ulm (2006):

$$\widehat{P(s)} = \frac{2\tan\theta}{\pi}E^{\mathrm{i}}_{\mathrm{pl}}(\widehat{K_{\mathrm{sl}}(s)},\widehat{G_{\mathrm{sl}}(s)},\varphi)\,\widehat{h^2(s)} \tag{14}$$

with $\widehat{P(s)}$ and $\widehat{h(s)}$ being the Laplace-transformed indentation force and indentation depth, respectively. $E^{\mathrm{i}}_{\mathrm{pl}}(\widehat{K_{\mathrm{sl}}(s)},\widehat{G_{\mathrm{sl}}(s)},\varphi)$ is the Laplace transformed indentation modulus. Introducing the relation between the modulus and the relaxation function from Eqs. (10) and (11) to the Laplace transformed indentation relaxation function $R^{\mathrm{i}}_{\mathrm{pl}}(\widehat{K_{\mathrm{sl}}(s)},\widehat{G_{\mathrm{sl}}(s)},\varphi)$, as follows:

$$R^{\mathrm{i}}_{\mathrm{pl}}(\widehat{K_{\mathrm{sl}}(s)},\widehat{G_{\mathrm{sl}}(s)},\varphi) = \frac{E^{\mathrm{i}}_{\mathrm{pl}}(\widehat{K_{\mathrm{sl}}(s)},\widehat{G_{\mathrm{sl}}(s)},\varphi)}{s}\,, \tag{15}$$

allows for rewriting Eq. (14) in a numerical convenient form:

$$\widehat{P(s)} = \frac{2\tan\theta}{\pi}R^{\mathrm{i}}_{\mathrm{pl}}(\widehat{K_{\mathrm{sl}}(s)},\widehat{G_{\mathrm{sl}}(s)},\varphi)\,s\widehat{h^2(s)}\,. \tag{16}$$

Transforming Eq. (16) back into the time domain yields the sought relaxation response of a conical indenter in a porous viscoelastic material, reading as:

$$P(t) = \frac{2\tan\theta}{\pi}\int_0^t R^{\mathrm{i}}_{\mathrm{pl}}(K_{\mathrm{sl}}(t-\tau),G_{\mathrm{sl}}(t-\tau),\varphi)\,\frac{\mathrm{d}}{\mathrm{d}\tau}h^2(\tau)\,\mathrm{d}\tau\,. \tag{17}$$

The method of functional equations requires the contact area to increase monotonically with time (Lee and Radok, 1960). Ting (1966) overcame this restriction and developed implicit equations for any load

history. Ting's solution is, however, rather challenging to employ (Vandamme and Ulm, 2006) and the presented method of functional equations is thus still commonly used for nanoindentation creep tests (Jäger et al., 2007; Kariem et al., 2020; Lu et al., 2003; Vandamme and Ulm, 2006) and relaxation tests (Ahmad et al., 2010; Ashrafi and Shariyat, 2010; Huang and Lu, 2007), and thus also employed herein. This way, the unloading phase is disregarded and specifying Eq. (17) for the loading ($0 \le t \le \tau_\mathrm{L}$) and holding ($\tau_\mathrm{L} < t \le \tau_\mathrm{H}$) indentation depth Eq. (1) leads to the following expressions for the force:

$$P(t) = \begin{cases} \frac{4\tan\theta}{\pi}\frac{h_\mathrm{max}^2}{\tau_\mathrm{L}^2}\int_0^t R_\mathrm{pl}^\mathrm{i}(K_\mathrm{sl}(t-\tau), G_\mathrm{sl}(t-\tau), \varphi)\,\tau\,\mathrm{d}\tau\,, & \forall \quad 0 \le t \le \tau_\mathrm{L} \\ \frac{4\tan\theta}{\pi}\frac{h_\mathrm{max}^2}{\tau_\mathrm{L}^2}\int_0^{\tau_\mathrm{L}} R_\mathrm{pl}^\mathrm{i}(K_\mathrm{sl}(t-\tau), G_\mathrm{sl}(t-\tau), \varphi)\,\tau\,\mathrm{d}\tau & \forall \quad \tau_\mathrm{L} < t \le \tau_\mathrm{H}. \end{cases} \tag{18}$$

Eq. (18) is the sought analytical solution of the relaxation behavior to the viscoelastic indentation tests performed by Schwaighofer et al. (2023). Before being able to evaluate the tests according to Eq. (18), we are left with discussing the indentation relaxation function of R_pl^i, dealt with hereafter.

2.7. Rheological models for solid lignin

We assume that the viscous deformations (the time-dependent part of the total deformations) of *solid* lignin are isochoric, i.e. viscous deformations are deviatoric only, and the volume remains constant during creep or relaxation processes. This assumption is motivated by similar assumptions for wood (Hofer et al., 2019), polymers (Beijer and Spoormaker, 2002; Hofer et al., 2019), and for the lignin–hemicellulose matrix considered as the source of viscous deformations in wood (Eitelberger et al., 2012). The bulk modulus of solid lignin is thus constant (time-independent), while the shear modulus remains time-dependent:

$$K_\mathrm{sl} = \mathrm{const}, \quad G_\mathrm{sl} = G_\mathrm{sl}(t). \tag{19}$$

We continue our development in the Laplace domain and recall that the Laplace transformed indentation relaxation function of porous lignin is defined as $\widehat{R_\mathrm{pl}^\mathrm{i}} = \widehat{E_\mathrm{pl}^\mathrm{i}}/s$ according to Eq. (15). Then, considering the isochoric behavior (19) in the expression of the homogenized indentation modulus Eq. (7) leads to the following expression of the relaxation indentation function in the Laplace domain:

$$\widehat{R_\mathrm{pl}^\mathrm{i}(s)} = \frac{\widehat{G_\mathrm{sl}(s)}(1-\varphi)(8\widehat{G_\mathrm{sl}(s)}+9K_\mathrm{sl})[32\widehat{G_\mathrm{sl}(s)}^2+9K_\mathrm{sl}^2(12+11\varphi)+12\widehat{G_\mathrm{sl}(s)}K_\mathrm{sl}(11+14\varphi)]}{s(4\widehat{G_\mathrm{sl}(s)}+3K_\mathrm{sl})(8\widehat{G_\mathrm{sl}(s)}+9K_\mathrm{sl}+12\widehat{G_\mathrm{sl}(s)}\varphi+6K_\mathrm{sl}\varphi)[8\widehat{G_\mathrm{sl}(s)}+3K_\mathrm{sl}(3+5\varphi)]}, \tag{20}$$

with $\widehat{G_\mathrm{sl}(s)}$ being the Laplace transform of the viscoelastic shear modulus of solid lignin, which is specified according to different rheological models hereafter.

In this study, three rheological models for solid lignin are investigated:

1. The Zener model is a linear 3-parameter model consisting of a spring in series with a Kelvin–Voigt element (spring and damper in parallel), see Fig. 4(a). The shear modulus in the Laplace domain reads as (Vandamme and Ulm, 2006):

$$\widehat{G_\mathrm{sl}(s)} = \left(\frac{1}{G_\mathrm{sl,0}} + \frac{1}{G_\mathrm{sl,V}+s\eta_\mathrm{sl,V}}\right)^{-1}, \tag{21}$$

where $G_\mathrm{sl,0}$ is the elastic shear modulus. $G_\mathrm{sl,V}$ and $\eta_\mathrm{sl,V}$ are the viscous shear modulus and the viscosity of the Kelvin–Voigt spring and dashpot, respectively. Notably, the deviatoric relaxation function of the Zener model reads as (Vandamme and Ulm, 2006):

$$R_\mathrm{sl}^\mathrm{dev}(t) = G_\mathrm{sl,0} - \frac{G_\mathrm{sl,0}^2}{G_\mathrm{sl,0}+G_\mathrm{sl,V}}\left[1-\exp\left(-\frac{(G_\mathrm{sl,0}+G_\mathrm{sl,V})t}{\eta_\mathrm{sl,V}}\right)\right]. \tag{22}$$

2. The linear 4-parameter Burgers model is obtained by combining a Maxwell element (spring and damper in series) and a Kelvin–Voigt element in series, see Fig. 4(b). The shear modulus in the Laplace domain reads as (Vandamme and Ulm, 2006):

$$\widehat{G_\mathrm{sl}(s)} = \left(\frac{1}{G_\mathrm{sl,0}} + \frac{1}{s\eta_\mathrm{sl,M}} + \frac{1}{G_\mathrm{sl,V}+s\eta_\mathrm{sl,V}}\right)^{-1}, \tag{23}$$

where $G_\mathrm{sl,0}$, $G_\mathrm{sl,V}$, and $\eta_\mathrm{sl,V}$ are denoted by analogy to the Zener model and $\eta_\mathrm{sl,M}$ is the viscosity of the Maxwell-dashpot. The corresponding relaxation function for the Burgers model reads as:

$$\begin{aligned} R_\mathrm{sl}^\mathrm{dev}(t) = \frac{G_\mathrm{sl,0}}{2B}\Big[&\exp\left((A-C)\frac{t}{2}\right)\left(\eta_\mathrm{sl,M}G_\mathrm{sl,0}+\eta_\mathrm{sl,V}G_\mathrm{sl,0}-\eta_\mathrm{sl,M}G_\mathrm{sl,V}+B\right) \\ &+\exp\left((A+C)\frac{t}{2}\right)\left(-\eta_\mathrm{sl,M}G_\mathrm{sl,0}-\eta_\mathrm{sl,V}G_\mathrm{sl,0}+\eta_\mathrm{sl,M}G_\mathrm{sl,V}+B\right)\Big] \end{aligned} \tag{24}$$

with

$$\begin{aligned} A &= -\frac{G_\mathrm{sl,0}}{\eta_\mathrm{sl,M}} - \frac{G_\mathrm{sl,0}}{\eta_\mathrm{sl,V}} - \frac{G_\mathrm{sl,V}}{\eta_\mathrm{sl,V}}, \\ B &= \sqrt{-4\eta_\mathrm{sl,M}\eta_\mathrm{sl,V}G_\mathrm{sl,0}G_\mathrm{sl,V} + (\eta_\mathrm{sl,M}G_\mathrm{sl,0}+\eta_\mathrm{sl,V}G_\mathrm{sl,0}+\eta_\mathrm{sl,M}G_\mathrm{sl,V})^2}, \\ \text{and } C &= \frac{B}{\eta_\mathrm{sl,M}\eta_\mathrm{sl,V}}. \end{aligned} \tag{25}$$

3. The modified power law (MPL) model is a 3-parameter model, see Fig. 4(c). Its relaxation function is typically defined in the time domain as (Bonfanti et al., 2020):

$$R_\mathrm{sl}^\mathrm{dev}(t) = G_\mathrm{sl,\infty} + \frac{G_\mathrm{sl,0}-G_\mathrm{sl,\infty}}{\left(1+\frac{t}{t_\mathrm{ref}}\right)^{\alpha_\mathrm{sl}}}, \tag{26}$$

where α_sl is the power law exponent and $t_\mathrm{ref} = 1\,\mathrm{s}$ is the reference time. $G_\mathrm{sl,0}$ is the instantaneous shear modulus and $G_\mathrm{sl,\infty}$ the shear modulus after infinite time. The sought shear modulus in the Laplace domain is gained from the corresponding Laplace-transformed relaxation function using the relationship $\widehat{G(s)} = s\widehat{R(s)}$, see Eq. (11), resulting in:

$$\widehat{G_\mathrm{sl}(s)} = G_\mathrm{sl,\infty} + s\,t_\mathrm{ref}(G_\mathrm{sl,0}-G_\mathrm{sl,\infty})\exp(s\,t_\mathrm{ref})E_{\alpha_\mathrm{sl}}(s\,t_\mathrm{ref}), \tag{27}$$

with E_{α_sl} as exponential integral function reading as:

$$E_{\alpha_\mathrm{sl}}(s\,t_\mathrm{ref}) = \int_1^\infty \frac{\exp(-s\,t_\mathrm{ref}\,t)}{t^{\alpha_\mathrm{sl}}}dt. \tag{28}$$

The elastic properties of solid lignin, specifically the shear modulus $G_\mathrm{sl,0}$ and the bulk modulus K_sl, are obtained from the Young's modulus and Poisson's ratio according to the linear elastic relations Eq. (5). The Young's modulus is obtained from the indentation modulus according to Eq. (4) by assuming a Poisson's ratio of 0.4, which is typical for polymers (Chemical Retrieval on the Web (CROW), 2023). Notably, a varying Poisson's ratio has only a minor effect on the indentation modulus. The indentation modulus, in turn, is determined by the Oliver–Pharr (Oliver and Pharr, 1992) method of the unloading curve, as it is commonly done in nanoindentation testings.

3. Results and discussion

3.1. Experimental observations

First, we qualitatively analyze the experimentally measured and averaged relaxation curves of (porous) lignin based on the averaged relaxation curves at indentation depths of 900 nm for all five lignins as seen in Fig. 5. We specifically focus on the decrease in force during

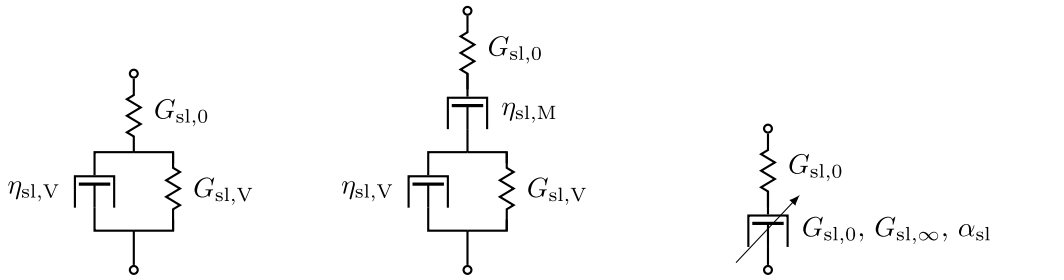

(a) Zener model (b) Burgers model (c) Modified power law (MPL) model

Fig. 4. Rheological models used to describe the viscoelastic properties of solid lignin.

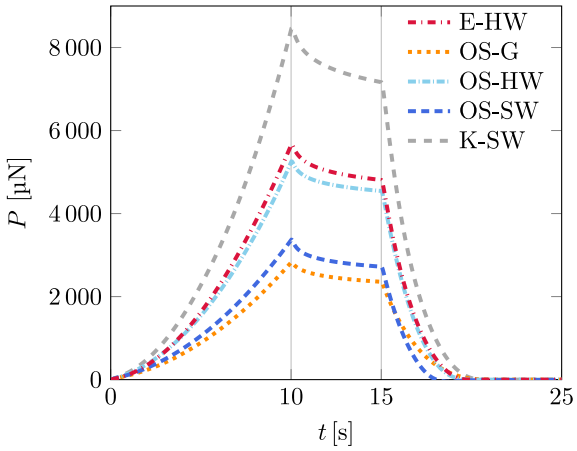

Fig. 5. Comparison of the experimentally measured relaxation curves for each lignin at a maximum indentation depth of 900 nm.

the holding phase at a constant indentation depth ($\tau_L \leq t \leq \tau_H$), as this period is less affected by potential plastic effects or damage, and thus reveals the material's relaxation behavior and viscoelasticity. The first notable observation is the rapid decrease in force at the beginning of the holding phase for all five tested lignins, indicating a rather pronounced short-term relaxation of lignin. Throughout the entire holding phase, the measured force continues to decrease, albeit at a diminishing rate.

The relaxation curves of all five lignins exhibit similar shapes. The curves mainly differ by the magnitude of the peak load and by the relaxation rate, whereby the lignins with high forces also exhibit larger relaxation rates. We recall that the measurements refer to porous lignin. This way, it is not surprising that the lignin with the smallest porosity exhibits the highest force and also the highest relaxation rate. Accounting for the porosity by means of micromechanics homogenization showed that the elastic modulus of all five tested lignins is relatively similar (Schwaighofer et al., 2023). Whether a similar conclusion can also be drawn regarding the viscous material properties will be explored in this paper, but this requires the evaluation and fitting of the modeled relaxation curves, which is dealt with in the following.

3.2. Evaluation and fitting

To evaluate the modeled relaxation curves, the Laplace-transformed indentation relaxation function of porous lignin $\widehat{R^i_{pl}(s)}$ according to Eq. (20) is specialized for the Laplace transformed shear modulus $\widehat{G_{sl}(s)}$ from either of the three rheological models [Eqs. (21), (23), or (27)] and the resulting expression is back-transformed into the time domain in order to obtain the analytical solution for the viscoelastic indentation problem in Eq. (18). As for the Zener and the Burgers model, this back-transformation can be performed analytically, resulting in an expression for the indentation force as a function of time t, porosity φ, indentation test parameters (h_{max}, τ_L, τ_H, θ), elastic parameters ($G_{sl,0}$, K_{sl}) and viscous parameters ($G_{sl,V}$, $\eta_{sl,V}$, $\eta_{sl,M}$). As for the MPL model, back-transformation is performed numerically by means of the Tablot algorithm (Abate and Whitt, 2006). In order to obtain the sought relaxation curve, the convolution integrals in Eq. (18) are solved by employing the trapezoidal rule.

Finally, the viscous parameters of solid lignin are fitted such that the modeled relaxation curve $P^{mod}(t)$ matches the experimentally measured (average) relaxation curve $P^{exp}(t)$ as closely as possible. We thereby focus on the holding phase ($\tau_L \leq t \leq \tau_H$), as this is the region where the relaxation curve is most sensitive to the viscous parameters. For fitting, an error ϵ is defined, reading as:

$$\epsilon = \frac{\sum_i^n [P^{mod}(t_i) - P^{exp}(t_i)]^2}{\sum_i^n [P^{exp}(t_i) - \overline{P}^{exp}(t_i)]^2} \quad \forall \quad \tau_L \leq t \leq \tau_H \,, \tag{29}$$

where $n = 501$ equidistant points during the holding period are evaluated. $\overline{P}^{exp}$ is the mean experimental force of the holding period. This error is minimized with the trust region algorithm (Branch et al., 1999; Byrd et al., 1988) implemented in Matlab to quantify the viscous parameters of the three different rheological models, specifically, $G_{sl,V}$ and $\eta_{sl,V}$ for the Zener model, $G_{sl,V}$, $\eta_{sl,V}$ and $\eta_{sl,M}$ for the Burgers model, and $G_{sl,\infty}$ and α_{sl} for the MPL model. This fitting procedure results in optimum viscous solid lignin parameters and corresponding errors ϵ, which are gathered in Table 2.

3.3. Comparison of rheological models

Comparing the fitting errors ϵ for each rheological model in Table 2, it is evident that the Burgers model provides the best representation of the experimental results with an average error over all lignins and depths of $\epsilon = 4.4 \times 10^{-3}$. The MPL model follows closely with $\epsilon = 7.7 \times 10^{-3}$, while the Zener model exhibits a significantly higher average error of $\epsilon = 13.3 \times 10^{-3}$. Notably, the MPL model achieves such a good performance with just two fitting parameters, one less than the Burgers model.

To delve deeper into the performance of the rheological models, we examine a representative relaxation curve (E-HW lignin at an indentation depth of 900 nm) more closely, see Fig. 6. Although only the holding period was used to fit the models, the loading path of all three models aligns well with the experimental results, as shown in Fig. 6a. Looking at the relaxation curve (Fig. 6b) and error (Fig. 6c) during the holding phase, we observe that the Burgers and MPL models are very close to the experimental measurements during the last 3.5 s of the holding period, where the error almost vanishes. The majority of the total error stems from the deviation at the beginning of the holding phase, where the initial relaxation in the experiment is stronger than in the models. In Section 3.4, we will discuss potential enhancements to the rheological model to capture this ultra-short-term relaxation. Notably, the first peak in the difference between the experiments and

Table 2
Oliver–Pharr-determined modulus $G_{sl,0}$ and fitting parameters of the rheological models (Zehner, Burgers, MPL) and corresponding errors ϵ for all lignins and indentation depths.

Lignin	h_{max}	OPM[a]	Zener model			Burgers model								MPL model		
	[nm]		2-parameter fit			3-parameter fit				4-parameter fit (see Section 3.4)				2-parameter fit		
		$G_{sl,0}$ [GPa]	$G_{sl,V}$ [GPa]	$\eta_{sl,V}$ [GPas]	ϵ [10^{-3}]	$G_{sl,V}$ [GPa]	$\eta_{sl,V}$ [GPas]	$\eta_{sl,M}$ [GPas]	ϵ [10^{-3}]	$G_{sl,0}$ [GPa]	$G_{sl,V}$ [GPa]	$\eta_{sl,V}$ [GPas]	$\eta_{sl,M}$ [GPas]	ϵ [10^{-3}]	$G_{sl,\infty}$ [GPa]	α_{sl} [–]	ϵ [10^{-3}]
E-HW	600	2.5	3.1	7.2	8.9	3.7	6.4	157.0	4.3	2.9	3.3	4.1	105.9	0.9	1.3	1.2	8.1
	900	2.4	2.6	5.9	12.3	3.3	5.0	119.2	2.7	2.7	3.0	3.7	95.5	0.9	1.2	1.3	4.9
	1000	2.2	2.4	5.5	11.5	3.0	4.7	109.6	3.2	2.5	2.7	3.3	84.7	0.9	1.1	1.3	5.7
OS-G	600	1.7	1.5	5.0	8.4	1.9	4.8	84.0	7.2	2.1	1.8	2.7	40.3	0.8	0.7	0.9	12.9
	900	3.1	4.1	11.6	9.1	4.9	11.2	278.5	8.2	3.9	4.4	5.4	117.2	0.9	1.5	0.9	14.3
	1000	1.8	2.1	5.4	10.1	2.5	5.0	110.8	7.5	2.2	2.2	2.7	61.8	1.1	0.9	1.0	12.6
OS-HW	600	2.6	3.1	6.5	11.7	3.8	5.7	157.5	3.7	3.0	3.3	3.9	118.5	1.0	1.3	1.4	6.7
	900	2.8	3.0	5.7	20.1	3.7	4.6	140.6	1.8	3.0	3.4	3.9	126.5	1.1	1.4	1.6	3.4
	1000	2.5	2.9	5.3	19.4	3.5	4.4	142.8	2.2	2.7	3.2	3.5	125.0	1.2	1.3	1.6	4.0
OS-SW	600	3.0	2.6	6.6	13.3	3.3	5.9	119.0	6.9	3.7	2.9	3.7	81.6	1.3	1.3	1.3	10.8
	900	2.8	2.0	4.6	21.3	2.6	3.8	85.6	3.8	3.3	2.4	3.0	72.2	1.6	1.1	1.6	6.1
	1000	3.8	3.6	8.0	14.6	4.5	6.9	167.3	4.3	4.5	4.0	4.9	129.7	1.2	1.7	1.4	7.1
K-SW	600	2.5	2.8	7.2	8.8	3.5	6.6	141.3	5.2	2.9	3.1	4.0	89.5	0.9	1.2	1.1	9.4
	900	3.0	3.5	8.6	9.9	4.5	7.4	141.3	2.7	3.4	4.1	5.2	110.6	0.8	1.5	1.1	4.8
	1000	2.0	1.7	3.9	20.1	2.3	3.1	68.0	2.0	2.2	2.1	2.6	60.7	1.1	0.9	1.5	3.7
mean		2.6			13.3				4.4	3.0	3.1	3.8	94.7	1.1			7.7

[a] Oliver–Pharr method (OPM).

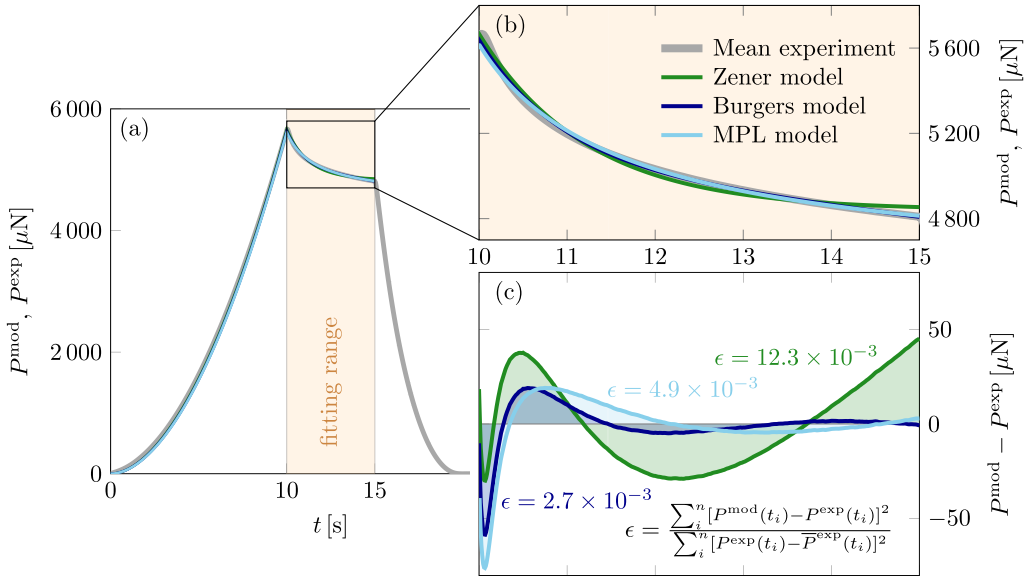

Fig. 6. Representative fit of the Zener, Burgers, and MPL model to the mean force–time curve of E-HW at $h_{max} = 900$ nm with (a) an overview of the whole experimental time range; (b) a detailed view of the holding period which was used to fit models to the experiment; (c) the difference of the force between the model P^{mod} and the experiment P^{exp} during the holding phase.

the model (Fig. 6c) does not precisely align with the beginning of the holding period. This shift is attributed to the precision limitations of the nanoindenter, which reaches the maximum displacement and therefore also the peak load somewhere between 10.0 s and 10.1 s. The model, however, is evaluated for a perfectly trapezoidal load history (Fig. 1) and a holding phase starting precisely at 10 s. The error resulting from this marginal mismatch is considered negligible.

We proceeded with our investigation of the viscous behavior of solid lignin by comparing the three fitted relaxation functions of the representative lignin (E-HW at $h_{max} = 900$ nm), shown in Fig. 7. All three relaxation functions start at the elastic shear stiffness $G_{sl,0} = 2.43$ GPa, followed by a very rapid decline, resembling the pronounced short-term relaxation of solid lignin. Already after five seconds, the relaxation function of the Zener model is very close to its asymptote (difference less than 1%) $G_{sl,\infty,Z} = \lim_{t\to\infty} R_{sl}^{dev}(t) = 1.27$ GPa. This explains the progressively growing error in Fig. 6 between the already practically constant Zener model response and the still decreasing experimentally measured relaxation behavior towards the end of the holding phase. The MPL model exhibits an asymptote at $G_{sl,\infty} = 1.19$ GPa, but it is approached much slower than in the case of the Zener model, such that the experimentally measured force decrease is well captured throughout the entire 15 s-indentation test. During the first 10 s, the Burgers model behaves similarly to the MPL model. Only thereafter, and thus outside the time frame investigated, do the respective relaxation functions diverge, as the Burgers relaxation function tends to zero at infinite time. Therefore, additional tests with longer holding times would be necessary to determine the longer-term viscoelastic response of solid hot-pressed lignin.

3.4. Capturing the short-term relaxation behavior

We now focus on improving the model performance during the beginning of the holding regime to better capture the severe short-term relaxation. A steeper decrease (more relaxation) of the force right after

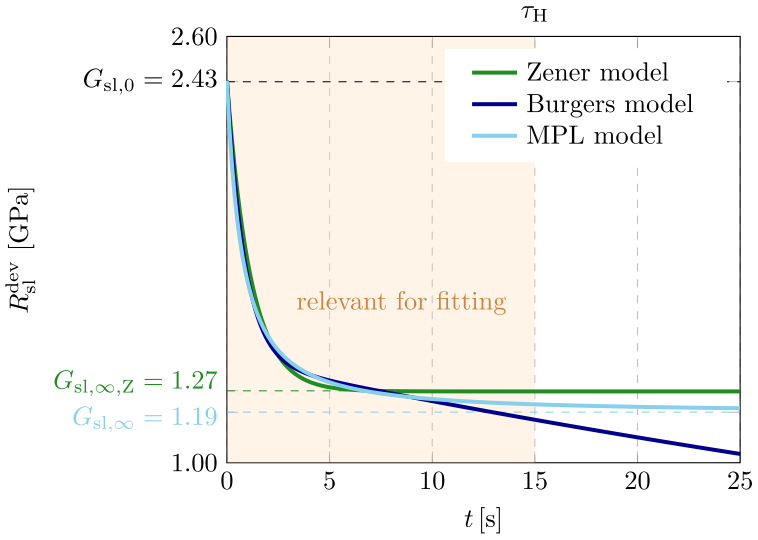

Fig. 7. Deviatoric relaxation functions of solid lignin from the representative fit of E-HW at $h_{max} = 900\,nm$. The corresponding model parameters are found in Table 2.

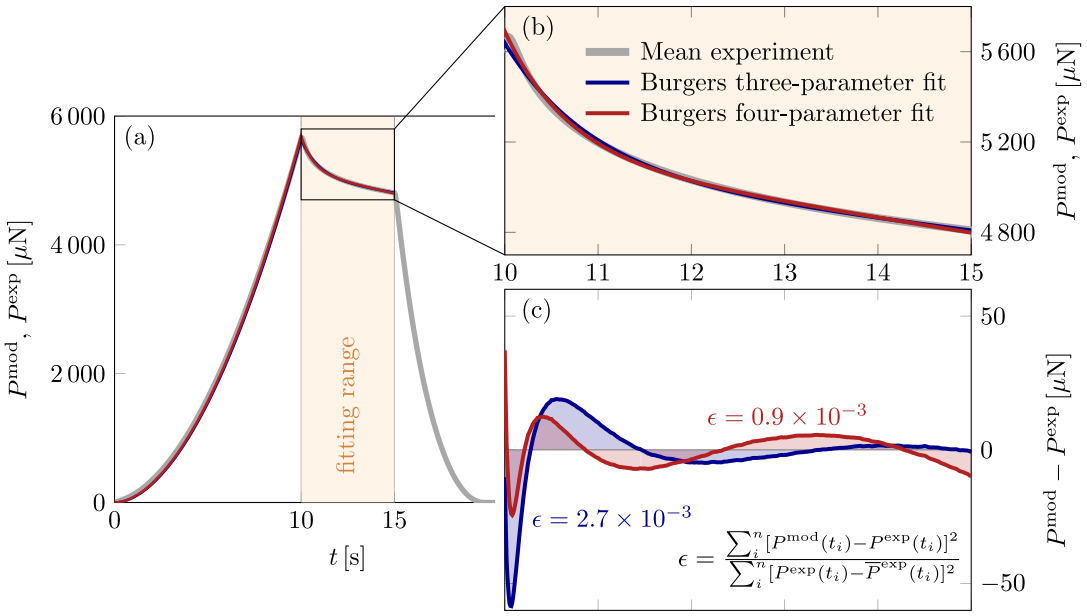

Fig. 8. Representative three-parameter ($G_{sl,V}$, $\eta_{sl,V}$, and $\eta_{sl,M}$) and four-parameter (E_{sl}, $G_{sl,V}$, $\eta_{sl,V}$, and $\eta_{sl,M}$) fit of the Burgers model to the mean force–time curve of E-HW at $h_{max} = 900\,nm$ with (a) an overview of the whole experimental time range; (b) a detailed view of the holding period which was used to fit the models to the experiment; (c) the difference of the force between the model P^{mod} and the experiment P^{exp} during the holding phase.

the start of the holding phase would be desirable, see the error peak in Fig. 6c. However, a more pronounced short-term relaxation would also decrease the predicted peak load at τ_L since, more force would relax during the loading, but this would contradict the experimentally measured peak load. An increase in the elastic stiffness would somewhat counteract this undesired effect and, together with a more pronounced short-term relaxation, would even better explain the observed force evolution. This is why, the elastic shear modulus of solid lignin $G_{sl,0}$ is considered as an additional fitting parameter, and a new and improved 4-parameter fit using the Burgers model is performed. Notably, the assumption of $\nu_{sl} = 0.4$ is maintained.

The 4-parameter Burgers model fit outperforms the three-parameter Burgers model fit, driven mainly by capturing the pronounced short-term relaxation at the beginning of the holding phase, see Fig. 8. The mean error, evaluated by averaging ϵ according to Eq. (29) over all lignins and indentation depths, reduces from 4.4×10^{-3} to 1.1×10^{-3}, see Table 2. Notably, the shear moduli, determined this way, are, on average, 16% larger than the moduli determined by the Oliver–Pharr method in the unloading branch (compare the corresponding columns in Table 2). In other words, in order to capture the short-term relaxation accurately, an increased shear stiffness is necessary, which is higher than the elastic unloading stiffness. This observation is in line with results from macroscopic creep tests on cementitious materials, which also indicated, that the unloading modulus (obtained from the unloading path of the force–displacement graph) significantly underestimates the modulus determined by fitting the entire creep behavior during the holding phase (Irfan-ul Hassan et al., 2016; Königsberger et al., 2021), albeit only by a few percent. We note that the actual stiffness of lignin, however, may be even slightly smaller than the Oliver–Pharr modulus, see the corrections proposed by Cheng et al. (2006), Ngan et al. (2005), and Vandamme and Ulm (2006).

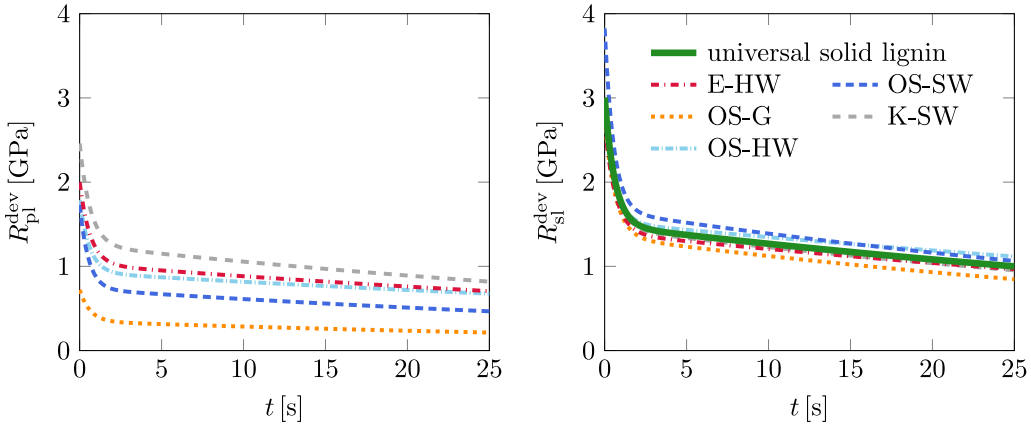

(a) Porous lignin (b) Solid lignin

Fig. 9. Relaxation functions obtained from the four-parameter Burgers model fit, averaged over all three indentation depths.

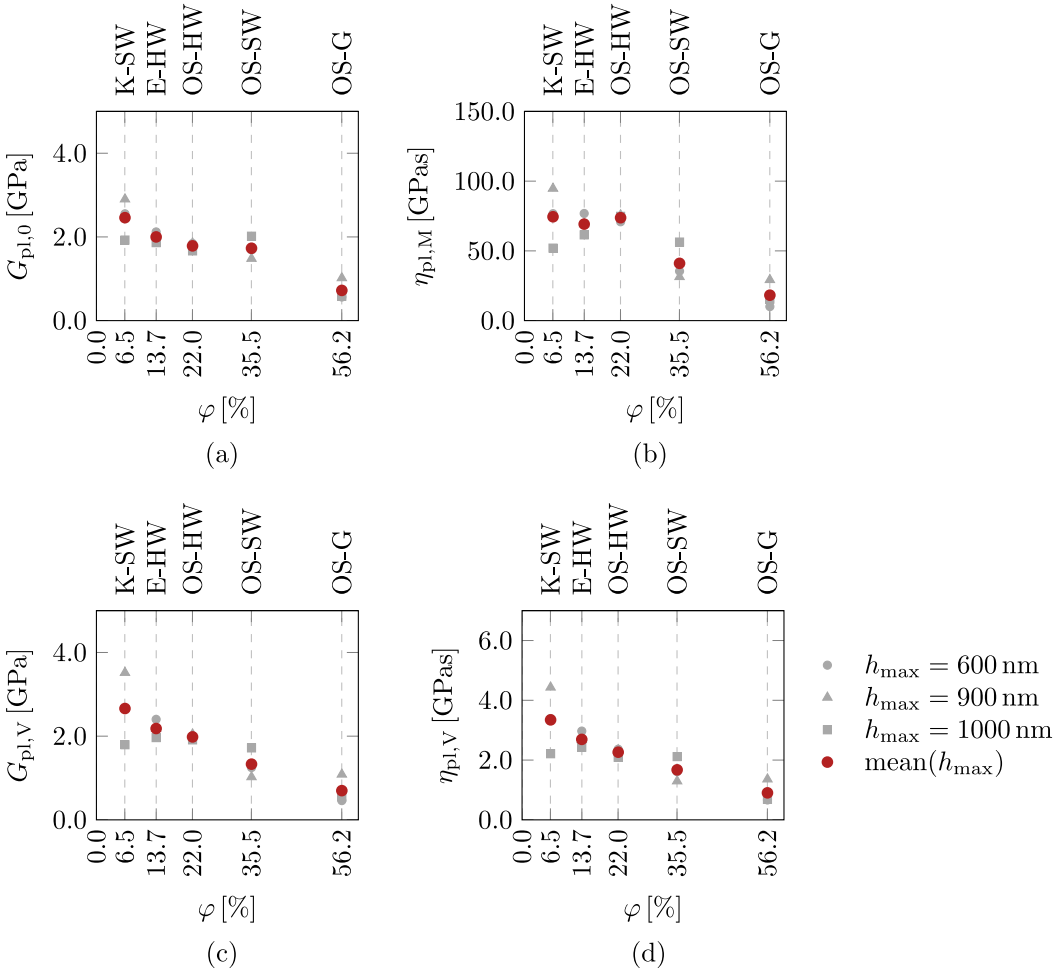

Fig. 10. Elastic (a) and viscous (b, c, and d) parameters of the Burgers model for porous lignin; gray points refer to specific indentation depths, and red points represent the average over the three different indentation depths. (For interpretation of the references to color in this figure legend, the reader is referred to the web version of this article.)

3.5. Comparison of different lignins

Finally, we compare the relaxation behavior of the five different lignins. Therefore, we rely on the fitting results of the 4-parameter Burgers fit, as this model results in the smallest average error. Relaxation curves (Fig. 9) of both solid and porous lignin are compared first. To obtain the relaxation function of porous lignin $R_{\mathrm{pl}}^{\mathrm{dev}}$, the bulk modulus of porous lignin K_{pl} Eq. (2) is considered constant and the shear modulus G_{pl} Eq. (3) is replaced with the Burgers model Eq. (23) in the Laplace domain. Considering these modifications, the Burgers model parameters of porous lignin are determined in the same manner as for solid lignin, by fitting the modeled force to the measured force during holding. As expected, the resulting relaxation functions $R_{\mathrm{pl}}^{\mathrm{dev}}$ of the five porous lignins are rather different for all five lignins, see

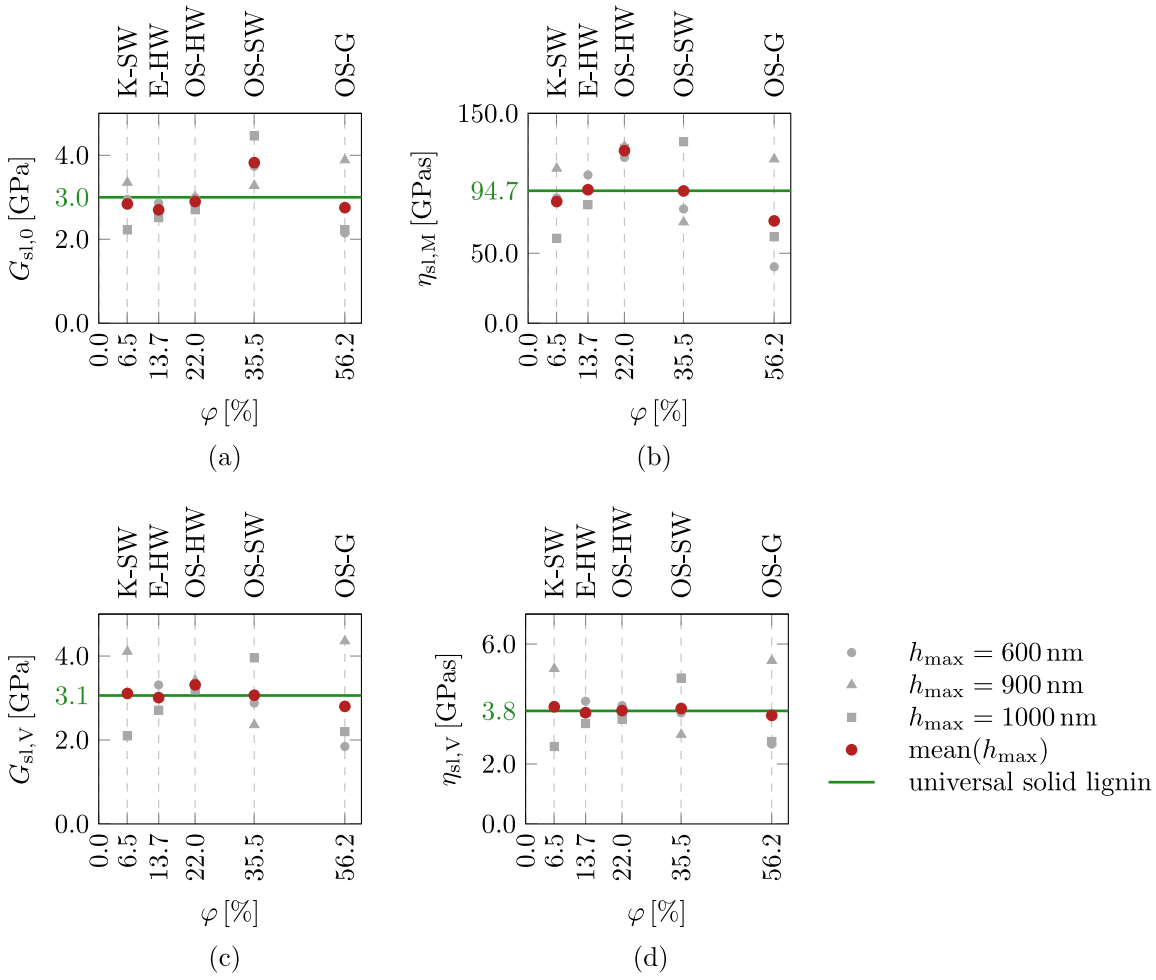

Fig. 11. Elastic (a) and viscous (b, c, and d) parameters of the Burgers model for solid lignin; gray points refer to specific indentation depths, red points represent the average over the three different indentation depths; the horizontal green line is the average over the red points and represents universal lignin parameters. (For interpretation of the references to color in this figure legend, the reader is referred to the web version of this article.)

Fig. 9(a). Most remarkably, the relaxation curves of the corresponding five solid lignins, R_{sl}^{dev}, in turn, practically follow a single master curve, see Fig. 9(b).

This result is further highlighted by studying the fitted Burgers model parameters of porous and solid lignin as a function of the porosity of the hot-pressed lignin samples, see Figs. 10 and 11. In this comparison, we included the results from the three different indentation depths (gray points) as well as a mean value (red points). The fitted parameters for the lignin pore composite increase with decreasing porosity tending towards the parameters of solid lignin. In contrast, the solid lignin parameters show only a minor variation among the different lignins. For the viscous parameters, $G_{sl,V}$ and $\eta_{sl,V}$, nearly constant solid lignin parameters emerge. Remarkably, even though the five solid lignin samples exhibit notable chemical distinctions (Klason lignin, ash, and carbohydrate content, as well as different monolignol profiles, see Table 1), they reveal similar viscoelastic behavior. This leads us to conclude that the viscoelastic material behavior of the *solid* lignin within the hot-pressed samples is practically independent of the origin of the lignin and, moreover, almost independent of the method used for lignin extraction. A similar conclusion, albeit only referring to the elastic modulus of solid lignin, was already given in Schwaighofer et al. (2023).

The practically constant viscoelastic behavior of the five tested solid lignins motivates the definition of a universal relaxation behavior of lignin produced under the conditions described in the Material section. The universal viscoelastic properties of solid lignin are obtained by averaging the parameters of all lignins and indentation depths (solid green line in Figs. 9 and 11). The resulting universal viscous Burgers model parameters are $G_{sl,V} = 3.1$ GPa, $\eta_{sl,V} = 3.8$ GPas, and $\eta_{sl,M} = 94.7$ GPas. The elastic part of the universal Burgers parameters can be expressed in the form of the shear $G_{sl,0} = 3.0$ GPa and the bulk modulus $K_{sl} = 14.0$ GPa, or equivalently as the elastic modulus $E_{sl} = 8.4$ GPa and the Poisson's ratio $\nu_{sl} = 0.4$.

The time-dependent relaxation phenomena observed in polymers arise from the dynamics of their long molecular chains. Under constant strain, these chains progressively rotate and unwind over time, leading to reduced stress levels (Brinson and Brinson, 2015). This viscoelastic response is strongly influenced by temperature and exhibits notable changes during the transition from the glassy state to the rubbery state. This transformation is characterized by the glass transition temperature, which varies between different lignins. Our nanoindentation tests show that, within the glassy state and at identical temperatures, our lignin samples exhibit comparable viscoelastic behavior. However, as temperatures approach the vicinity of the glass transition temperature, there might be an escalation in the differentiation of viscoelastic properties between the various lignin types.

4. Conclusions

Reevaluation of over 6000 nanoindentation relaxation tests conducted on five hot-pressed lignins, extracted from various feedstocks

by using different extraction methods, has yielded the following conclusions:

- Lignin is a viscoelastic material, and its relaxation behavior exhibits a pronounced short-time response in nanoindentation tests.
- Reliable viscoelastic parameters of solid (i.e., pore-free) lignin could be deduced from nanoindentation relaxation tests on porous lignin samples. This is achieved by adopting the method of functional equations together with micromechanics-based homogenization theory.
- Accounting for the production-induced porosity reveals that the viscoelastic behavior of solid (i.e., pore-free) lignin, produced by hot-pressing at 90 °C and 108 MPa, is practically independent of both the feedstock (softwood, hardwood, grass) and the lignin extraction process (organosolv, kraft pulping, enzymatic hydrolysis)
- The observed viscoelastic behavior of solid lignin can be accurately modeled as an isochoric material with a constant bulk modulus of $K_{sl} = 14.0$ GPa and a time-dependent shear behavior resembled by a four-parameter Burgers model with the moduli $G_{sl,0} = 3.0$ GPa and $G_{sl,V} = 3.1$ GPa and with viscosities $\eta_{sl,V} = 3.8$ GPas and $\eta_{sl,M} = 94.7$ GPas.
- In addition, this work integrates an analytical homogenization approach into the identification of viscoelastic behavior, from nanoindentation experiments, by means of three different rheological models using the method of functional equations in a concise manner.

CRediT authorship contribution statement

Michael Schwaighofer: Methodology, Writing – original draft, Visualization, Formal analysis. **Markus Königsberger:** Writing – original draft, Methodology. **Luis Zelaya-Lainez:** Investigation, Resources. **Markus Lukacevic:** Writing – review & editing, Funding acquisition, Supervision, Conceptualization, Project administration. **Sebastián Serna-Loaiza:** Resources, Writing – review & editing. **Michael Harasek:** Supervision. **Florian Zikeli:** Resources, Writing – review & editing. **Anton Friedl:** Supervision. **Josef Füssl:** Writing – review & editing, Supervision, Funding acquisition, Conceptualization, Project administration.

Declaration of competing interest

The authors declare that they have no known competing financial interests or personal relationships that could have appeared to influence the work reported in this paper.

Data availability

Data will be made available on request.

Acknowledgments

The funding from the Austrian Science Fund (FWF) through the START grant Y1093 “Virtual Wood Labs” and SFB F77 “Advanced Computational Design” is gratefully acknowledged. Furthermore, the financial support from the Austrian Federal Ministry of Labour and Economy, the National Foundation for Research, Technology and Development, Austria, and the Christian Doppler Research Association is gratefully acknowledged.

References

Abate, J., Whitt, W., 2006. A unified framework for numerically inverting Laplace transforms. INFORMS J. Comput. 18 (4), 408–421. http://dx.doi.org/10.1287/ijoc.1050.0137.

Ahmad, M.R., Nakajima, M., Kojima, S., Homma, M., Fukuda, T., 2010. Nanoindentation methods to measure viscoelastic properties of single cells using sharp, flat, and buckling tips inside ESEM. IEEE Trans. NanoBiosci. 9 (1), 12–23. http://dx.doi.org/10.1109/TNB.2009.2034849.

Akter, S.T., Binder, E., Bader, T.K., 2023. Moisture and short-term time-dependent behavior of Norway spruce clear wood under compression perpendicular to the grain and rolling shear. Wood Mater. Sci. Eng. 18 (2), 580–593. http://dx.doi.org/10.1080/17480272.2022.2056715.

Amin, A.F.M.S., Alam, M.S., Okui, Y., 2002. An improved hyperelasticity relation in modeling viscoelasticity response of natural and high damping rubbers in compression: experiments, parameter identification and numerical verification. Mech. Mater. 34 (2), 75–95. http://dx.doi.org/10.1016/S0167-6636(01)00102-8.

Asawaworarit, P., Daorattanachai, P., Laosiripojana, W., Sakdaronnarong, C., Shotipruk, A., Laosiripojana, N., 2019. Catalytic depolymerization of organosolv lignin from bagasse by carbonaceous solid acids derived from hydrothermal of lignocellulosic compounds. Chem. Eng. J. 356, 461–471. http://dx.doi.org/10.1016/j.cej.2018.09.048.

Ashrafi, H., Shariyat, M., 2010. A nanoindentation modeling of viscoelastic creep and relaxation behaviors of ligaments mechanical characteristics of biological tissues. In: 2010 17th Iranian Conference of Biomedical Engineering. ICBME, pp. 1–5. http://dx.doi.org/10.1109/ICBME.2010.5705019.

Bajwa, D.S., Pourhashem, G., Ullah, A.H., Bajwa, S.G., 2019. A concise review of current lignin production, applications, products and their environmental impact. Ind. Crops Prod. 139, 111526. http://dx.doi.org/10.1016/j.indcrop.2019.111526.

Baker, D.A., Gallego, N.C., Baker, F.S., 2012. On the characterization and spinning of an organic-purified lignin toward the manufacture of low-cost carbon fiber. J. Appl. Polym. Sci. 124 (1), 227–234. http://dx.doi.org/10.1002/app.33596.

Beijer, J.G.J., Spoormaker, J.L., 2002. Solution strategies for FEM analysis with nonlinear viscoelastic polymers. Comput. Struct. 80 (14), 1213–1229. http://dx.doi.org/10.1016/S0045-7949(02)00089-5.

Benveniste, Y., 1987. A new approach to the application of Mori-Tanaka’s theory in composite materials. Mech. Mater. 6 (2), 147–157. http://dx.doi.org/10.1016/0167-6636(87)90005-6.

Bian, H., Jiao, L., Wang, R., Wang, X., Zhu, W., Dai, H., 2018. Lignin nanoparticles as nano-spacers for tuning the viscoelasticity of cellulose nanofibril reinforced polyvinyl alcohol-borax hydrogel. Eur. Polym. J. 107, 267–274. http://dx.doi.org/10.1016/j.eurpolymj.2018.08.028.

Bonfanti, A., Kaplan, J.L., Charras, G., Kabla, A., 2020. Fractional viscoelastic models for power-law materials. Soft Matter 16 (26), 6002–6020. http://dx.doi.org/10.1039/d0sm00354a.

Branch, M.A., Coleman, T.F., Li, Y., 1999. A subspace, interior, and conjugate gradient method for large-scale bound-constrained minimization problems. SIAM J. Sci. Comput. 21 (1), 1–23. http://dx.doi.org/10.1137/S1064827595289108.

Brinson, H.F., Brinson, L.C., 2015. Characteristics, applications and properties of polymers. In: Brinson, H.F., Brinson, L.C. (Eds.), Polymer Engineering Science and Viscoelasticity: an Introduction. Springer US, Boston, MA, pp. 57–100. http://dx.doi.org/10.1007/978-1-4899-7485-3_3.

Byrd, R.H., Schnabel, R.B., Shultz, G.A., 1988. Approximate solution of the trust region problem by minimization over two-dimensional subspaces. Math. Program. 40 (1), 247–263. http://dx.doi.org/10.1007/BF01580735.

Chemical Retrieval on the Web (CROW), 2023. Typical Poisson’s ratios of polymers at room temperature. URL: https://polymerdatabase.com/polymer%20physics/Poisson%20Table.html.

Cheng, Y.-T., Cheng, C.-M., Ni, W., 2006. Methods of obtaining instantaneous modulus of viscoelastic solids using displacement-controlled instrumented indentation with axisymmetric indenters of arbitrary smooth profiles. Mater. Sci. Eng. A-Struct. Mater. Proper. Microstruct. Process. 423 (1), 2–7. http://dx.doi.org/10.1016/j.msea.2005.09.134.

Chio, C., Sain, M., Qin, W., 2019. Lignin utilization: A review of lignin depolymerization from various aspects. Renew. Sustain. Energy Rev. 107, 232–249. http://dx.doi.org/10.1016/j.rser.2019.03.008.

Cousins, W.J., 1976. Elastic modulus of Lignin as related to moisture content. Wood Sci. Technol. 10 (1), 9–17.

Davydov, D., Jirásek, M., 2008. Modeling of nanoindentation by a visco-elastic porous model with application to cement paste. In: Nanotechnology in Construction: Proceedings of the NICOM3. Springer, pp. 187–192. http://dx.doi.org/10.1007/978-3-642-00980-8_25.

Donnelly, E., Baker, S.P., Boskey, A.L., Van Der Meulen, M.C., 2006. Effects of surface roughness and maximum load on the mechanical properties of cancellous bone measured by nanoindentation. J. Biomed. Mater. Res. - A 77 (2), 426–435. http://dx.doi.org/10.1002/jbm.a.30633.

Ebers, L.-S., Arya, A., Bowland, C.C., Glasser, W.G., Chmely, S.C., Naskar, A.K., Laborie, M.-P., 2021. 3D printing of lignin: Challenges, opportunities and roads onward. Biopolymers 112 (6), e23431. http://dx.doi.org/10.1002/bip.23431.

Eitelberger, J., Bader, T.K., de Borst, K., Jäger, A., 2012. Multiscale prediction of viscoelastic properties of softwood under constant climatic conditions. Comput. Mater. Sci. 55, 303–312. http://dx.doi.org/10.1016/j.commatsci.2011.11.033.

Gangwar, T., Schillinger, D., 2019. Microimaging-informed continuum micromechanics accurately predicts macroscopic stiffness and strength properties of hierarchical plant culm materials. Mech. Mater. 130, 39–57. http://dx.doi.org/10.1016/j.mechmat.2019.01.009.

Gindl, W., Gupta, H.S., Schöberl, T., Lichtenegger, H.C., Fratzl, P., 2004. Mechanical properties of spruce wood cell walls by nanoindentation. Appl. Phys. A 79 (8), 2069–2073. http://dx.doi.org/10.1007/S00339-004-2864-Y.

Habibi, M.K., Tam, L.-h., Lau, D., Lu, Y., 2016. Viscoelastic damping behavior of structural bamboo material and its microstructural origins. Mech. Mater. 97, 184–198. http://dx.doi.org/10.1016/j.mechmat.2016.03.002.

Hagen, R., Salmén, L., Stenberg, B., 1996. Effects of the type of crosslink on viscoelastic properties of natural rubber. J. Polym. Sci. B: Polym. Phys. 34 (12), 1997–2006. http://dx.doi.org/10.1002/(SICI)1099-0488(19960915)34:12<1997::AID-POLB5>3.0.CO;2-N.

Irfan-ul Hassan, M., Pichler, B., Reihsner, R., Hellmich, C., 2016. Elastic and creep properties of young cement paste, as determined from hourly repeated minute-long quasi-static tests. Cem. Concr. Res. 82, 36–49. http://dx.doi.org/10.1016/j.cemconres.2015.11.007.

Henriksson, G., 2009. Lignin. In: Wood Chemistry and Wood Biotechnology. Vol. 1. Walter de Gruyter, Berlin, New York, pp. 121–146. http://dx.doi.org/10.1515/9783110213409.121.

Hess, K.M., Killgore, J.P., Srubar, W.V., 2018. Nanoscale hygromechanical behavior of lignin. Cellulose 25 (11), 6345–6360. http://dx.doi.org/10.1007/S10570-018-2045-3.

Hilburg, S.L., Elder, A.N., Chung, H., Ferebee, R.L., Bockstaller, M.R., Washburn, N.R., 2014. A universal route towards thermoplastic lignin composites with improved mechanical properties. Polymer 55 (4), 995–1003. http://dx.doi.org/10.1016/j.polymer.2013.12.070.

Hofer, U., Pichler, C., Maderebner, R., Lackner, R., 2019. Lomnitz-type viscoelastic behavior of clear spruce wood as identified by creep and relaxation experiments: influence of moisture content and elevated temperatures up to 80 °C. Wood Sci. Technol. 53 (4), 765–783. http://dx.doi.org/10.1007/s00226-019-01099-8.

Huang, G., Lu, H., 2007. Measurements of two independent viscoelastic functions by nanoindentation. Exp. Mech. 47 (1), 87–98. http://dx.doi.org/10.1007/s11340-006-8277-4.

Jäger, A., Lackner, R., Eberhardsteiner, J., 2007. Identification of viscoelastic properties by means of nanoindentation taking the real tip geometry into account. Meccanica 42 (3), 293–306. http://dx.doi.org/10.1007/S11012-006-9041-7.

Kariem, H., Füssl, J., Kiefer, T., Jäger, A., Hellmich, C., 2020. The viscoelastic behaviour of material phases in fired clay identified by means of grid nanoindentation. Constr. Build. Mater. 231, 117066. http://dx.doi.org/10.1016/j.conbuildmat.2019.117066.

Königsberger, M., Honório, T., Sanahuja, J., Delsaute, B., Pichler, B.L., 2021. Homogenization of nonaging basic creep of cementitious materials: A multiscale modeling benchmark. Constr. Build. Mater. 290, http://dx.doi.org/10.1016/j.conbuildmat.2021.123144.

Königsberger, M., Lukacevic, M., Füssl, J., 2023. Multiscale micromechanics modeling of plant fibers: Upscaling of stiffness and elastic limits from cellulose nanofibrils to technical fibers. Mater. Struct. 56 (1), 13. http://dx.doi.org/10.1617/s11527-022-02097-2.

Lakes, R.S., 1998. Viscoelastic Solids. CRC Press, Boca Raton, http://dx.doi.org/10.1201/9781315121369.

Lee, H.J., Lee, H.K., Lim, E., Song, Y.S., 2015. Synergistic effect of lignin/polypropylene as a compatibilizer in multiphase eco-composites. Compos. Sci. Technol. 118, 193–197. http://dx.doi.org/10.1016/j.compscitech.2015.08.018.

Lee, E.H., Radok, J.R.M., 1960. The contact problem for viscoelastic bodies. J. Appl. Mech. 27 (3), 438–444. http://dx.doi.org/10.1115/1.3644020.

Lu, H., Wang, B., Ma, J., Huang, G., Viswanathan, H., 2003. Measurement of creep compliance of solid polymers by nanoindentation. Mech. Time-Depend. Mater. 7 (3), 189–207. http://dx.doi.org/10.1023/B:MTDM.0000007217.07156.9b.

Marcuello, C., Foulon, L., Chabbert, B., Aguié-Béghin, V., Molinari, M., 2020. Atomic force microscopy reveals how relative humidity impacts the Young's modulus of lignocellulosic polymers and their adhesion with cellulose nanocrystals at the nanoscale. Int. J. Biol. Macromol. 147, 1064–1075. http://dx.doi.org/10.1016/J.IJBIOMAC.2019.10.074.

Mori, T., Tanaka, K., 1973. Average stress in matrix and average elastic energy of materials with misfitting inclusions. Acta Metall. 21 (5), 571–574. http://dx.doi.org/10.1016/0001-6160(73)90064-3.

Ngan, A.H., Wang, H.T., Tang, B., Sze, K.Y., 2005. Correcting power-law viscoelastic effects in elastic modulus measurement using depth-sensing indentation. Int. J. Solids Struct. 42 (5–6), 1831–1846. http://dx.doi.org/10.1016/j.ijsolstr.2004.07.018.

Oliver, W., Pharr, G., 1992. An improved technique for determining hardness. J. Mater. Res. 7 (6), 1564–1583. http://dx.doi.org/10.1557/JMR.1992.1564.

Olsson, A.-M., Salmén, L., 1992. Viscoelasticity of in situ lignin as affected by structure. In: Viscoelasticity of Biomaterials. In: ACS Symposium Series, vol. 489, American Chemical Society, pp. 133–143. http://dx.doi.org/10.1021/bk-1992-0489.ch009.

Plomion, C., Leprovost, G., Stokes, A., 2001. Wood formation in trees. Plant Physiol. 127 (4), 1513–1523. http://dx.doi.org/10.1104/pp.010816.

Puxkandl, R., Zizak, I., Paris, O., Keckes, J., Tesch, W., Bernstorff, S., Purslow, P., Fratzl, P., 2002. Viscoelastic properties of collagen: synchrotron radiation investigations and structural model. Philos. Trans. R. Soc. Lond. Ser. B Biol. Sci. 357 (1418), 191–197. http://dx.doi.org/10.1098/rstb.2001.1033.

Radok, J.R.M., 1957. Visco-elastic stress analysis. Quart. Appl. Math. 15 (2), 198–202.

Rubio-Valle, J.F., Valencia, C., Sánchez, M., Martín-Alfonso, J.E., Franco, J.M., 2023. Oil structuring properties of electrospun Kraft lignin/cellulose acetate nanofibers for lubricating applications: influence of lignin source and lignin/cellulose acetate ratio. Cellulose 30 (3), 1553–1566. http://dx.doi.org/10.1007/s10570-022-04963-2.

Salmén, L., 1984. Viscoelastic properties ofin situ lignin under water-saturated conditions. J. Mater. Sci. 19 (9), 3090–3096. http://dx.doi.org/10.1007/BF01026988.

Schniewind, A.P., Barrett, J.D., 1972. Wood as a linear orthotropic viscoelastic material. Wood Sci. Technol. 6 (1), 43–57. http://dx.doi.org/10.1007/BF00351807.

Schwaighofer, M., Zelaya-Lainez, L., Königsberger, M., Lukacevic, M., Serna-Loaiza, S., Harasek, M., Lahayne, O., Senk, V., Füssl, J., 2023. Characterization of mechanical properties of five hot-pressed lignins extracted from different feedstocks by microscopy-aided nanoindentation. Mater. Des. 227, 111765. http://dx.doi.org/10.1016/j.matdes.2023.111765.

Sluiter, A., Hames, B., Ruiz, R., Scarlata, C., Sluiter, J., Templeton, D., 2012. Technical Report NREL/TP-510-42618: Determination of Structural Carbohydrates and Lignin in Biomass. Technical Report, National Renewable Energy Laboratory, Golden, Colorado, p. 15.

Sneddon, I.N., 1965. The relation between load and penetration in the axisymmetric boussinesq problem for a punch of arbitrary profile. Internat. J. Engrg. Sci. 3 (1), 47–57. http://dx.doi.org/10.1016/0020-7225(65)90019-4.

Tian, Z., He, J., Wang, Y., Zhao, W., Duan, L., 2022. Quantitative insights into rheology of self-crosslinking dialdehyde carboxymethyl cellulose/collagen solution: A comprehensive experimental and modelling investigation. Mech. Mater. 170, 104356. http://dx.doi.org/10.1016/j.mechmat.2022.104356.

Ting, T.C.T., 1966. The contact stresses between a rigid indenter and a viscoelastic half-space. J. Appl. Mech. 33 (4), 845–854. http://dx.doi.org/10.1115/1.3625192.

Tuck, C.O., Pérez, E., Horváth, I.T., Sheldon, R.A., Poliakoff, M., 2012. Valorization of biomass: Deriving more value from waste. Science 337 (6095), 695–699. http://dx.doi.org/10.1126/science.1218930.

Vandamme, M., Ulm, F.J., 2006. Viscoelastic solutions for conical indentation. Int. J. Solids Struct. 43 (10), 3142–3165. http://dx.doi.org/10.1016/J.IJSOLSTR.2005.05.043.

Watkins, D., Nuruddin, M., Hosur, M., Tcherbi-Narteh, A., Jeelani, S., 2015. Extraction and characterization of lignin from different biomass resources. J. Mater. Res. Technol. 4 (1), 26–32. http://dx.doi.org/10.1016/j.jmrt.2014.10.009.

Windeisen, E., Wegener, G., 2012. Lignin as building unit for polymers. In: Polymer Science: A Comprehensive Reference, 10 Volume Set. Vol. 10. Elsevier, pp. 255–265. http://dx.doi.org/10.1016/B978-0-444-53349-4.00263-6.

Xu, G., Wang, H., Zhu, H., 2017. Rheological properties and anti-aging performance of asphalt binder modified with wood lignin. Constr. Build. Mater. 151, 801–808. http://dx.doi.org/10.1016/j.conbuildmat.2017.06.151.

Zhang, T., Bai, S.L., Zhang, Y.F., Thibaut, B., 2012. Viscoelastic properties of wood materials characterized by nanoindentation experiments. Wood Sci. Technol. 46 (5), 1003–1016. http://dx.doi.org/10.1007/s00226-011-0458-3.